INTERNATIONAL JOURNAL OF HYDROGEN ENERGY 39 (2014) 20105–20115

Available online at www.sciencedirect.com

ScienceDirect

journal homepage: www.elsevier.com/locate/he

Influence of pH value on the structure and electronic property of the passive film on 316L SS in the simulated cathodic environment of proton exchange membrane fuel cell (PEMFC)

D.G. Li[*], *J.D. Wang*, *D.R. Chen*

State Key Laboratory of Tribology, Tsinghua University, Beijing, 100084, China

ARTICLE INFO

Article history:
Received 15 March 2014
Received in revised form
21 July 2014
Accepted 17 September 2014
Available online 25 October 2014

Keywords:
Proton exchange membrane fuel cells
Cathodic environment
316L stainless steel
pH value

ABSTRACT

The influence of pH value on the electronic property of the passive film on 316L SS in the simulated cathodic environment of the proton exchange membrane fuel cell (PEMFC), was investigated by potentiodynamic polarization curve, electrochemical impedance spectra and Mott–Schottky plot. The pH value effect on the composition and structure of the passive film on 316L SS was detected by X-ray photoelectron spectroscopy (XPS). The results showed that the passivity of 316L SS was enhanced, the transfer resistance of the film/solution interface significantly increased with the increase in pH value. Mott–Schottky analysis revealed that the passive film on 316L SS appeared a p-n heterojunction, the donor and acceptor densities within the passive film decreased, and the flat band potential moved to the positive direction with the increment of pH value. XPS results implied that the thickness of the passive film increased with increasing pH value. The passive film on 316L SS exhibited the duplex structure, in which the outer film was mainly composed of Cr-oxide and the inner film was dominantly consisted of Fe-oxides when the pH value was less than 3. In the case of pH $5H_2SO_4$ solution, Fe-oxides were the major component throughout the inner and outer films.

Introduction

Bipolar plates (BP) are the key components of proton exchange membrane fuel cell (PEMFC), which constituting over 80% of the total weight and about 30%–45% of the total cost in PEMFC [1,2]. High electrical conductivity, chemical stability, gas impermeability, good mechanical performance, easy to fabrication, and low cost are the desired properties of BP, but fewer materials can meet all the requirements. Stainless steel is recognized as the good candidate of BP [3–6] owing to the several merits including good mechanical strength, high electrical conductivity, high gas impermeability, low cost, and easy to fabrication. A lot of papers have been focused on the corrosion behaviors of stainless steels in the simulated PEMC cathodic environments [4,7–9], various results are obtained by different researchers owing to the different cathodic environments are chosen. Generally, the cathodic environments

* *Corresponding author*. Tel.: +86 10 6279 5148; fax: +86 10 6278 1379.
E-mail address: dgli@mail.tsinghua.edu.cn (D.G. Li).

http://dx.doi.org/10.1016/j.ijhydene.2014.09.089

of PEMFC are weekly acidic with a large region of pH value, the 0.5 M H_2SO_4 solution @70 °C, 1 M H_2SO_4 solution +2 ppm F^- @70 °C, 12.5 ppm H_2SO_4 solution +1.8 ppm HF @25 °C and 70 °C and the 5×10^{-4} M H_2SO_4 + 10 g·L^{-1} Na_2SO_4 solution can may be the cathodic environment in different references [4,7–9]. In spite of large interests focusing on the corrosion behaviors of stainless steel in the cathodic environments of PEMFC, as far as we know only one paper [10] has been published on the influence of pH on the electronic property and structure of the passive films on 316L SS. Even so, the insight influence of pH value on the structure and the electronic property of the passive films on 316L SS are not systemically obtained.

In this report the pH value effect on the electronic property and structure of the passive films on 316L SS in the cathodic environment of PEMFC is investigated by potentiodynamic polarization curve, electrochemical impedance spectra (EIS), Mott–Schottky plot and X-ray photoelectron spectroscopy (XPS).

Experimental

Material and electrolyte

The experimental material is prepared by manufacturing 316L SS in a form of wafer (Φ10 × 5 mm), in which the chemical composition of 316L SS is list in Table 1. One end surface of the wafer exposed in the electrolyte acted as the working surface is abraded with 2000 grit SiC paper, polished with 0.5 μm Al_2O_3 powder and then cleaned using double-distilled water, while other surfaces are sealed with epoxy resin in the lower part of an L-shaped glass tube.

The studied electrolyte are the H_2SO_4 solutions with different pH values, pre-bubbling is carried out for 1 h before each measurement and the solution is bubbled with air during measurement.

Electrochemical and XPS measurements

All electrochemical experiments are performed in a conventional three-electrode cell, the counter and reference electrodes are a platinum mesh and SCE electrode, respectively. All potentials mentioned in this paper are referred as the reference electrode.

Potentiodynamic polarization curve is carried out in the potential region from −0.25 V_{OCP} to 1.2 V_{SCE} with the scanning rate of 2 mV/s.

EIS apparatus is consisted of EG&G instrument model 273 A electrochemical working station with 5210 frequency response analyzer, the potential is increased by 10 mV and the sweeping frequency is from 100 kHz to 5 mHz.

Mott–Schottky plots of the passive films are also carried out at EG&G instrument model 273 A electrochemical working station with a 10 mV s^{-1} scanning rate, the scanning potential range is ranging from −0.2 V to 2 V, and the measured frequency is discussed in section 3.4.

XPS measurement is carried out at a PHI model 5400 X-ray photoelectron spectrometer, a Mg Ka source (1253.6 eV) is employed for all studies at a beam voltage of 15 kV and a source power of 400 W. The analyzed area is always 1 mm^2. Typical operating pressure is $2–4 \times 10^{-9}$ Torr.

Table 1 – Chemical composition of 316L SS (wt.%).

Fe	Cr	Ni	Mo	Si	Cu	Other
66.3	16.9	12.5	2.23	0.52	0.5	Balance

Results and discussions

Influence of pH value on the potentiodynamic curves of 316L SS in H_2SO_4 solution

The potentiodynamic polarization responses of 316L SS in H_2SO_4 solutions with different pH values at 25 °C, are showed in Fig. 1. It can be observed that 316L SS behaves the passive character in H_2SO_4 solution, in which the steady passive potential region for 316L SS in pH1 H_2SO_4 solution is extended from −0.14 V_{SCE} to 0.81 V_{SCE}. The steady passive current density, i_{ss}, reaches to the order of the magnitude of 10^{-5} A·cm^{-2}, and i_{ss} decreases with the increment of pH value, implying the enhanced passivity of 316L SS in H_2SO_4 solution with increasing pH value. The passive current density sharply increases with the potential moving from 0.81 V_{SCE} to 1.08 V_{SCE} (point a), and the passive current density turns to decrease in the potential region from 1.08 V_{SCE} (point a) to 1.45 V_{SCE} (point b). The variation of the passive current density in the potential region from 0.81 V_{SCE} to 1.45 V_{SCE} (point b) is related to the passive-transpassive transition. The values of the related electrochemical parameters, i.e., the corrosion potential (E_{corr}), the corrosion current density (i_{corr}), the steady passive current density (i_{ss}), the anodic Tafel slope (β_a) and the cathodic Tafel slope (β_c) are acquired by fitting the potentiodynamic curves, and the results are list in Table 2. As shown in Table 2, the cathodic Tafel slope (β_c) decreases from −101.7 to −577.18 mV·dec^{-1}, whereas the anodic Tafel slope (β_a) increases with increasing pH value. The corrosion potential (E_{corr}) shifts to positive direction, and the corrosion current density (i_{ss}) decreases with the increase in pH value, which implies the increment of pH value has a protective affect on the anti-corrosion performance of 316L SS in H_2SO_4 solution.

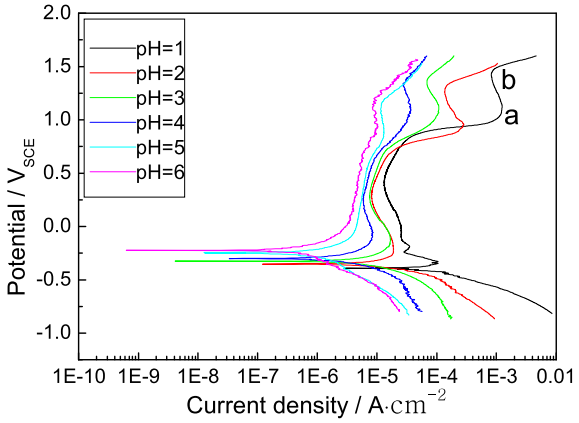

Fig. 1 – The passive behaviors of 316L stainless steel in H_2SO_4 solution with different pH values at 25 °C.

Table 2 – Electrochemical parameters extracted from potentiodynamic curves of 316L SS in H_2SO_4 solution with different pH values at 25 °C.

Solutions	β_a/mV·decade^{-1}	β_c/mV·decade^{-1}	E_{corr}/V_{SCE}	i_{corr}/A·cm^{-2}	i_{ss}/A·cm^{-2}
pH = 1	121.6	−101.7	−0.386	1.09e-5	1.88e-5
pH = 2	206.39	−191.2	−0.354	7.34e-6	1.14e-5
pH = 3	487.4	−331.14	−0.326	5.66e-6	1e-5
pH = 4	556.9	−378.2	−0.301	4.17e-6	7.41e-6
pH = 5	676.8	−423.44	−0.244	3.39e-6	5.69e-6
pH = 6	883.2	−577.18	−0.23	1.25e-6	4.91e-6

Influence of pH value on XPS of the passive films on 316L at 0.6 V for 24 h in H_2SO_4 solution

The chemical compositions of the passive films on 316L SS in the simulated cathodic environment of PEMFCS are detected by XPS. Fig. 2 shows the survey XPS of the passive films on 316L SS at 0.6 V for 24 h in H_2SO_4 solutions with different pH values, it is seen that the passive film is mainly composed of C, O, Ni, Cr, Fe and Mo, in which C comes from pollution and Fe_3C. As 316L SS is the austenite stainless steel, Fe_3C appeared in the passive film may originate from the substrate cementite. O, Ni, Cr, Fe and Mo originate from the oxides in the passive film. As shown in Fig. 2, the Cr_{2p} intensity decreases and the Fe_{2p} intensity sharply increases with the increment of pH value. Especially in the case of pH $5H_2SO_4$ solution, the intensity of Fe_{2p} peak reaches to the maximum, indicating the dependence of the film composition on the pH value. Fig. 3 shows the XPS depth profiles of Cr, Fe, Ni, Mo, O and C elements in the passive films on 316L SS at 0.6 V for 24 h in H_2SO_4 solutions with different pH values, it can be seen that there is no obvious difference existed in the variations of Cr, Fe, Ni, Mo, O and C with pH value in the case of every pH value. The oxygen atomic concentration reaches to the maximum at the depth of 1 nm, and it sharply decreases to a constant value. The carbon atomic concentration sharply decreases to a constant concentration within the depth of 3 nm. Cr, Fe, Mo and Ni atomic concentrations increase with the increment of depth and then they reach to a constant value. Additionally,

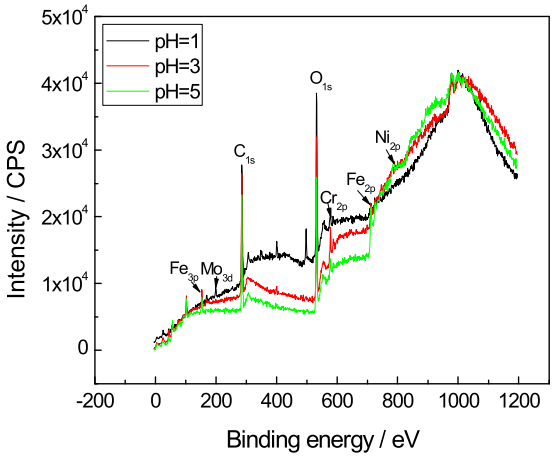

Fig. 2 – Survey XPS of the passive films on 316L stainless steel at 0.6 V for 24 h in H_2SO_4 solutions with different pH values.

Fig. 3(a and b) shows that the Cr atomic concentration is higher than Fe atomic concentration when the sputtering depth is below 1.87 nm. Then, Fe atomic concentration starts sharply to increase, and the Cr atomic concentration is initially lower than that of Fe when the sputtering depth is over 1.87 nm. While in the case of pH5, the Fe atomic concentration is consistently higher than the Cr atomic concentration in the total sputtering depth. The above illustrations indicate that the passive film on 316L SS in pH1 or $3H_2SO_4$ solution appears the duplex structure, in which the outer film is mainly composed of Cr-oxide, and Fe-oxides is the major component of the inner film. However, the Fe-oxides become the major component throughout the inner and outer film when pH value is 5. Unfortunately, the XPS finding is inconsistent with the composition and structure of the passive film on stainless steel reported by the previous papers [11–15]. In order to verify the above illustration, the variation of the Fe/Cr atomic concentration ration with the depth is depicted in Fig. 3(d), it can be observed that the Fe/Cr ration increases with increasing depth in the case of pH1 or pH3, the Fe/Cr ration is over 1 when the sputtering depth is over 2.43 nm. The Fe/Cr ration in the case of pH3 is bigger than that in the case of pH1, implying the increased Fe concentration in the passive film with the increase in pH value. While in the case of pH5, the Fe/Cr ration initially decreases from 2.47 to 1.46, then it rapidly increases from 1.46 to 3.65 when the sputtering depth is over 5 nm. But the Fe/Cr ration is still over 1.0, which implying the major component of the passive film is Fe-oxides throughout the inner and outer films. The film thickness is estimated to the distance from film surface to the position where the major oxide content is around 20% [10]. Accordingly, the passive film formed on 316L SS at 0.6 V for 24 h in the simulated cathodic environment of PEMFC, is estimated to be of 5.26 nm in the case of pH1, and it increases to 6 nm and 7.98 nm in the cases of pH3 and pH5, respectively. Obviously, the film thickness increases with the increment of pH value, it is accordance with the previous paper [10].

For sake of exploring the pH value effect on the chemical composition of the passive film on 316L SS, Fig. 4 gives the narrow spectra of Cr_{2p}, Fe_{2p}, Ni_{2p}, Mo_{3d}, O_{1s} and C_{1s} of the passive film formed in pH1 H_2SO_4 solution, and the narrow XPS is measured after sputtering for 1 nm. Fig. 4(a) is the Cr_{2p} narrow spectra measured after sputtering for 1.0 nm depth in the case of pH1, it can be observed that the $Cr_{2p3/2}$ peaks have been systematically decomposed into five components. One locates at a biding energy of 576.88 eV, and four others locate at BEs of 575.44 eV, 574.4 eV, 573.66 eV and 573.05 eV, respectively. These BEs are close to the BEs of $Cr_{2p3/2}$ in Cr_2O_3,

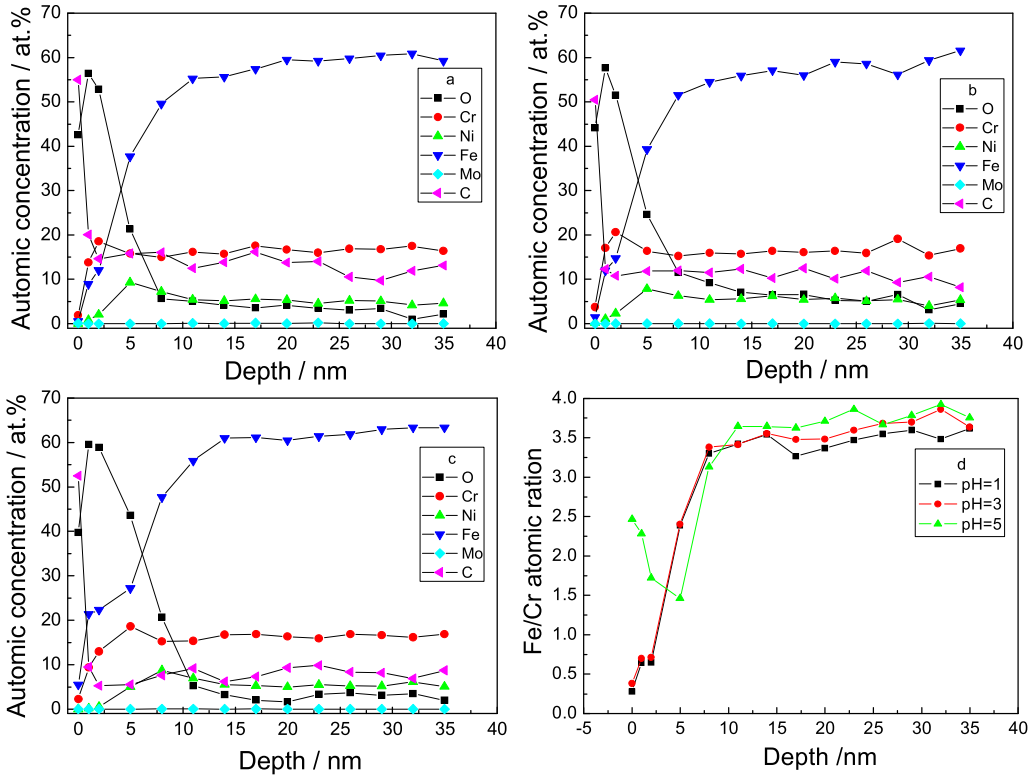

Fig. 3 – XPS depth profiles of Cr, Fe, Ni, Mo, O and C elements in the passive films on 316L SS at 0.6 V for 24 h in H_2SO_4 solutions with different pH values, a) pH = 1, b) pH = 3, c) pH = 5, and d) Fe/Cr ration.

CrO_3^{2-} and Cr. The $Fe_{2p3/2}$ peaks can be decomposed into six components, and the corresponding BEs of six components are located at 707 eV, 707.85 eV, 708.85 eV, 709.54 eV, 710.32 eV and 711.25 eV, respectively. These BEs are closed to the BEs of $Fe_{2p3/2}$ in Fe, Fe_3C, FeO, Fe_2O_3 and FeOOH, respectively. Fig. 4(c) shows that $Ni_{2p3/2}$ spectra can be divided into three peaks, the corresponding BEs are 852.16 eV, 852.57 eV and 853.24 eV, respectively. These BEs are near to the BEs of $Ni_{2p3/2}$ in Ni and NiO. Only one decomposed peak with the corresponded BE of 232.36 eV appears in the $Mo_{3d5/3}$ narrow spectra, the BE of 232.36 eV is close to the BE of $Mo_{3d5/3}$ in MoO_3. For the O_{1s} narrow spectra, it can be seen that six decomposed peaks appear, their BEs are close to the BEs of O_{1s} in FeO, Fe_2O_3, MoO_2, Cr_2O_3 and MoO_3, respectively. While for the C_{1s} narrow spectra, three peaks appear, and their BEs are 283.97 eV, 284.92 eV and 285.56 eV, respectively. These BEs are close to the BEs of C_{1s} in Fe_3C and C, respectively.

Similarly, Fig. 5 shows the narrow spectra of Cr_{2p}, Fe_{2p}, Ni_{2p}, Mo_{3d}, O_{1s} and C_{1s} of the passive film formed in pH 3 H_2SO_4 solution, and the narrow XPS is also measured after sputtering for 1 nm. It can be observed that Cr appears in the passive film in the form of Cr_2O_3 and $Cr(OH)_3$; Fe exists in the passive film in the feature of Fe-oxides, FeOOH and Fe_3C; Ni appears in the form of NiO and Ni_2O_3; Mo appears in the feature of MoO_2 and MoO_3; C exists in the passive film in the form of Fe_3C and C. While for O element, it is seen that O can come from Cr_2O_3, Fe_2O_3, Ni_2O_3 and MoO_3.

When the pH value is increased to 5, the composition and structure of the passive film formed on 316L SS in pH5 H_2SO_4 solution may be changed. It can be seen from Fig. 6(a) that the Cr_{2p} narrow spectra measured after sputtering for 8.0 nm depth can be systematically decomposed into four components. The corresponded BEs are 574.16 eV, 575.97 eV, 576.87 eV and 577.82 eV, respectively. These BEs are close to the BEs of $Cr_{2p3/2}$ in Cr, CrO_2^{2-}, Cr_2O_3 and CrO_4^-, respectively. Fig. 6(b) shows that the $Fe_{2p3/2}$ peaks can be decomposed into five components, and the corresponding BEs are 706.49 eV, 706.95 eV, 707.63 eV, 708.68 eV and 710.5 eV, respectively. These BEs are closed to the BEs of $Fe_{2p3/2}$ in Fe, Fe_3O_4 and Fe_3O_4, respectively. Fig. 6(c) shows that $Ni_{2p3/2}$ spectra can be divided into three peaks, the corresponding BEs are 852.71 eV, 853.11 eV and 853.77 eV, respectively. These BEs are near to the BEs of $Ni_{2p3/2}$ in Ni and NiO. Two decomposed peaks with the corresponded BEs of 226.33 eV and 231.42 eV appear in the $Mo_{3d5/3}$ narrow spectra, the BE of 226.33 eV is close to the BE of $Mo_{3d5/3}$ in Mo, and the BE of 231.42 eV is close to the BE of $Mo_{3d5/3}$ in MoO_3. For the O_{1s} narrow spectra, it can be seen that six decomposed peaks appear, their BEs are 529.6 eV, 530.01 eV, 530.43 eV, 530.87 eV, 531.42 eV and 532.38 eV, respectively. These BEs are close to the BEs of O_{1s} in NiO, FeO, Fe_2O_3, MoO_3 and Cr_2O_3, respectively. While for the C_{1s} narrow spectra, three decomposed peaks with the corresponded BEs of 282.99 eV, 284.6 eV and 285.54 eV appear, these BEs are close to the C_{1s} in C and its satellites.

Additionally, it can be observed from Figs. 4b and 5b that the intensities of Fe-oxides increase with increasing pH value. The Fe-oxides intensities showed in Fig. 5(e) are bigger than the Fe-oxides intensities depicted in Fig. 4(e), which verifying

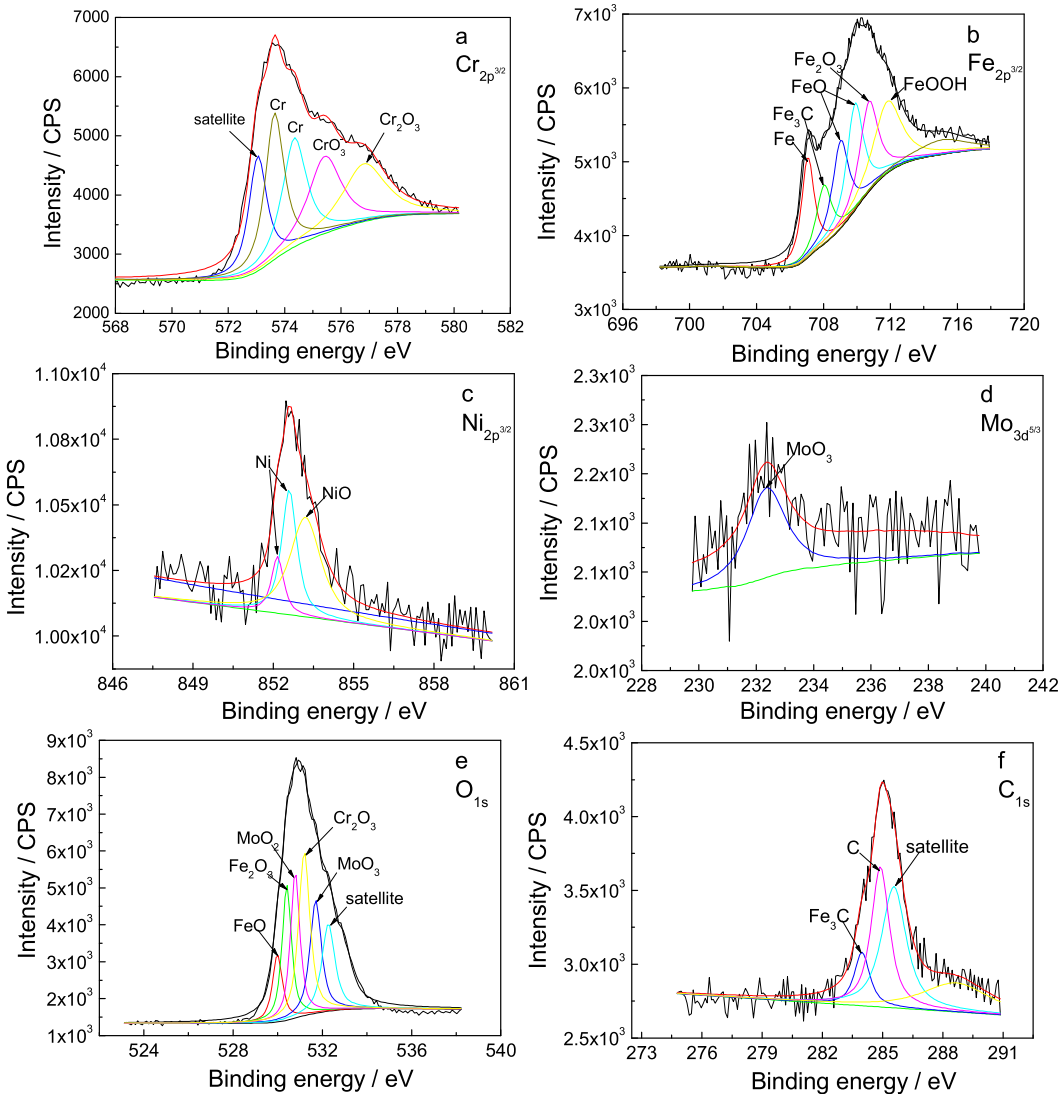

Fig. 4 – Narrow spectra of Cr_{2p}, Fe_{2p}, Ni_{2p}, Mo_{3d}, O_{1s} and C_{1s} of the passive film on 316L SS at 0.6 V for 24 h in pH 1 H_2SO_4 solution, a) Cr_{2p}, b) Fe_{2p}, c) Ni_{2p}, d) Mo_{3d}, e) O_{1s}, and f) C_{1s}, in which the sputtering depth is 1 nm.

the increased Fe-oxide content in the passive film with increasing pH value. For the appearance of Fe_3C, the intensity of $Fe_{2p3/2}$ in Fe_3C sharply decreases with increasing pH value (see Figs. 4b and 5b, 4f and 5f), and it disappears when the pH value increases to 5 (see Fig. 6(b and f)).

Influence of pH value on EIS of the passive films on 316L at 0.6 V for 24 h in H_2SO_4 solution

To insight into the influence of pH value on the electronic property of the passive film on 316L SS, Fig. 7 displays the Nyquist plots and the corresponded Bode diagrams of the passive films on 316L SS at 0.6 V_{SCE} for 24 h, respectively. It can be seen that the Nyquist plots the passive films show a depressed semicircle, and the presence of the depressed semicircles is often referred to as frequency dispersion, which has been attributed to high roughness or inhomogeneity of the electrode surface [16,17]. Evidently, the diameters of the capacitive arcs enlarge with increasing pH value, suggesting the great improvement of the film protectiveness with increasing pH value. The Bode diagram of 316L SS in the case of pH1 H_2SO_4 shows the typical of passive feature, characterized by the phase angles approaching −80° in a broad frequency range. In cases of pH2 H_2SO_4, the constant phase angle increases, but the corresponded frequency range significantly decreases. In cases of pH3, 4, 5 and 6 H_2SO_4, the constant phase angle continues to increase, and the corresponded frequency range sharply decreases with increasing pH value. While the phase angle within the high frequency range keeps a low constant, and the corresponded high frequency range enlarges with increasing pH value, implying the increased solution resistance with increasing pH value.

In order to gain the quantitative explain of pH value on the electronic property of the passive film on 316L SS, the measured EIS are fitted by appropriate equivalent electron circuit using ZsimpWin software. The equivalent electron circuit with three hierarchically distributed time constants provided by Macdonald [18] (show in Fig. 8) is used to fit the

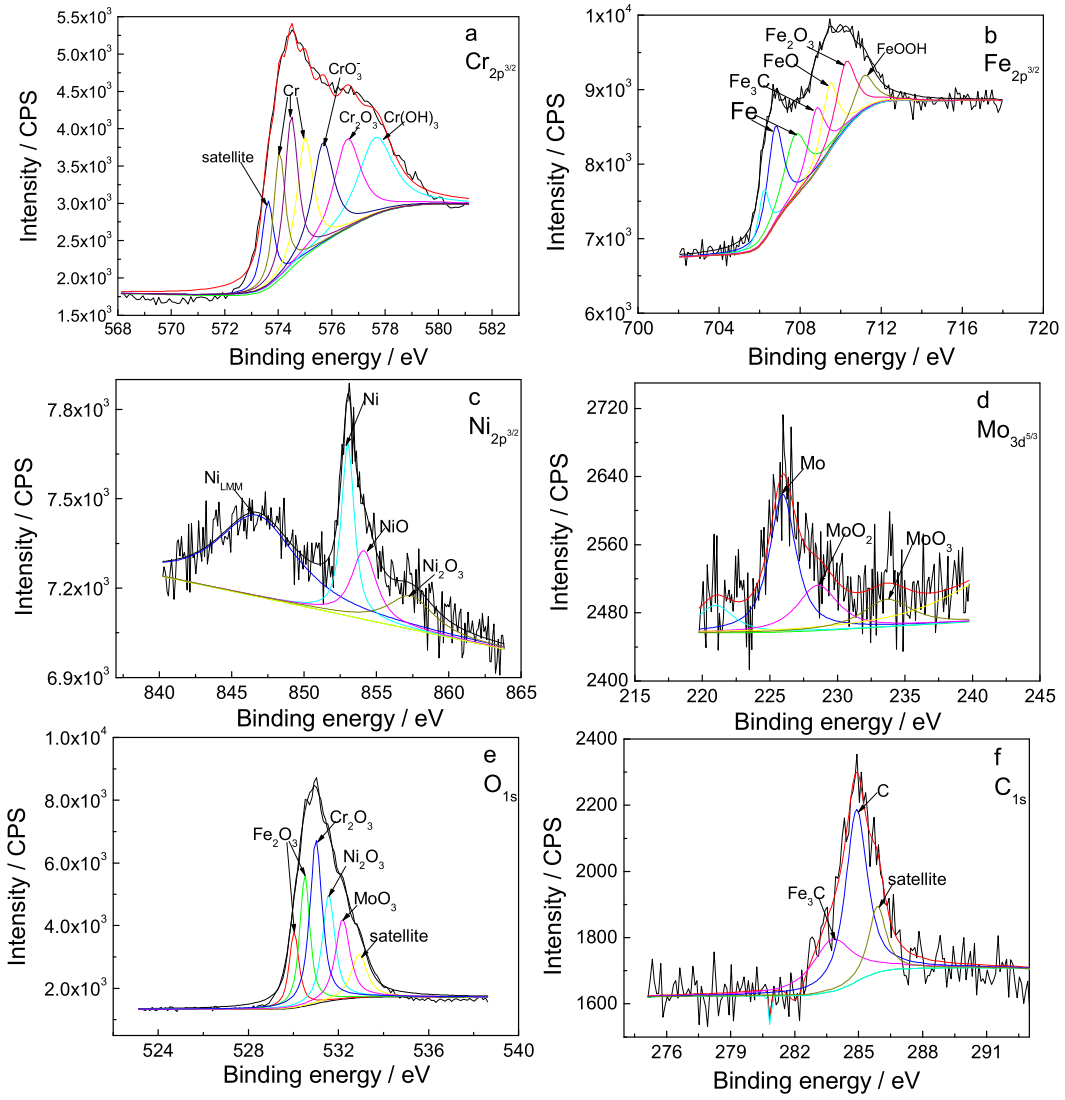

Fig. 5 – Narrow spectra of Cr_{2p}, Fe_{2p}, Ni_{2p}, Mo_{3d}, O_{1s} and C_{1s} of the passive film on 316L SS at 0.6 V for 24 h in pH $3H_2SO_4$ solution, a) Cr_{2p}, b) Fe_{2p}, c) Ni_{2p}, d) Mo_{3d}, e) O_{1s}, and f) C_{1s}, in which the sputtering depth is 1 nm.

impedance, in which C_1 and R_1 represent the capacitive and resistive contributions of the metal/film interface, C_f and R_f represent the capacitance and resistance of the bulk passive film, R_2 and CPE (constant phase element) represent the solution/barrier interface, and R_s is the solution resistance. The CPE has the properties of a capacitance when $0.5 < n < 1$. Frequency dispersion leading to CPE behavior can be attributed to geometry-induced nonuniform current [19,20] and potential distribution (2D distribution) or to charge–discharge of oxide layers [21,22] or to porosity or to surface roughness [23,24] (3D distribution). For blocking electrode, the impedance of the CPE can be obtained with the following relationship [25,26]:

$$Z_{CPE} = R + \frac{1}{(j2\pi f)^n Y} \quad (1)$$

Where j is the imaginary number, and f is the frequency of the alternative current. Y and n are constants, where $n = 1$, Y has unit of a capacitance, i.e., uF/cm^2, and represents the capacity of the interface. When $n = 0$, the CPE is an ideal resistor. When $n = 0.5$, the CPE represents the Warburg impedance with diffusion character.

Table 3 summarizes the fitting results, the chi-squared (χ^2) values of the order of 10^{-3} ~ 10^{-5} indicating satisfactory agreement between the experimental and simulated data. The fitting results shows that the value of α is in the range of 0.79 and 0.91 for all the fitted results, validating the association of the CPE to a frequency disperse electrode. The total resistance (ΣR) significantly increases with the increase in pH value, while the values of C_1, C_f and Q degrade, implying of the enhanced film protection with pH value. The increased total resistance with pH value can be contributed to resistive changing occurring at the film/solution and metal/film interfaces. It can be seen from Table 3 that the value of R_2 is much higher than that of R_1 or R_f in the case of every pH value, and R_2 increases with the increase in pH value, considering R_2

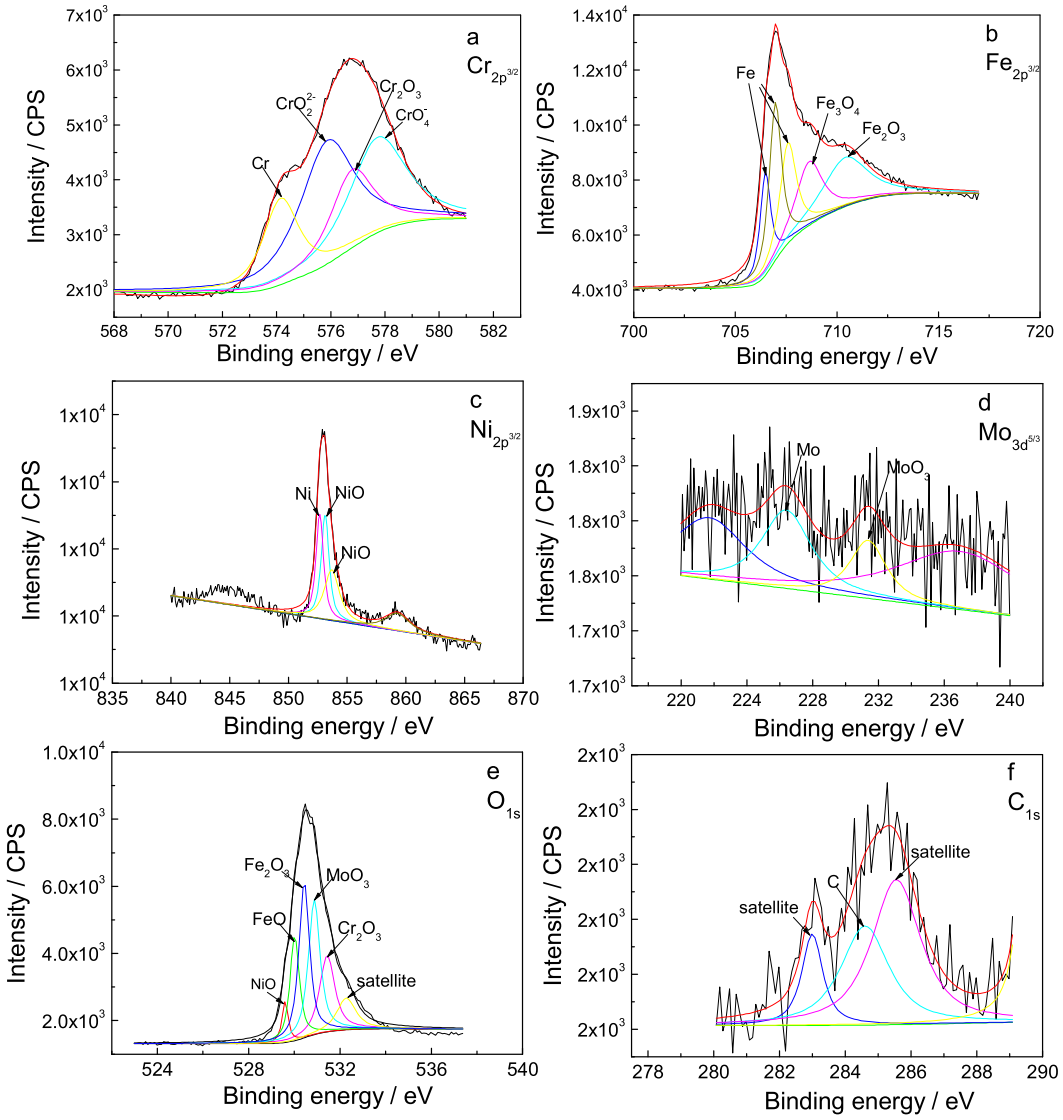

Fig. 6 – Narrow spectra of Cr_{2p}, Fe_{2p}, Ni_{2p}, Mo_{3d}, O_{1s} and C_{1s} of the passive film on 316L SS at 0.6 V for 24 h in pH 3 H_2SO_4 solution, a) Cr_{2p}, b) Fe_{2p}, c) Ni_{2p}, d) Mo_{3d}, e) O_{1s}, and f) C_{1s}, in which the sputtering depth is 8 nm.

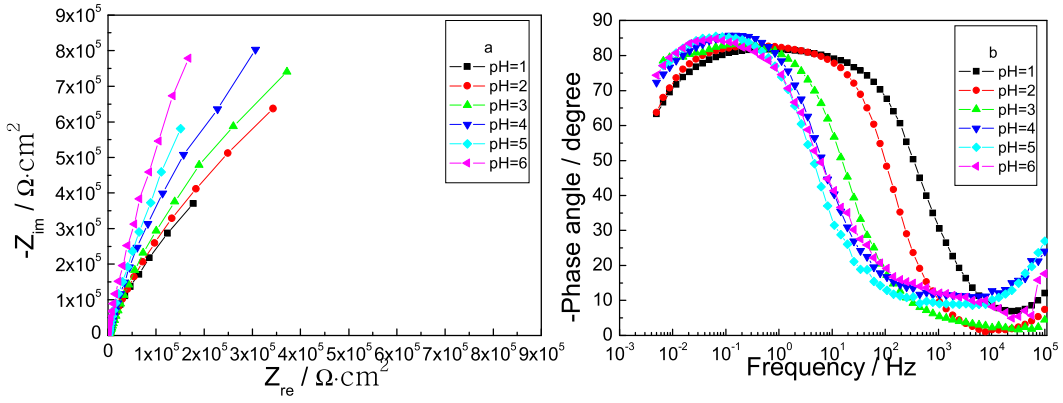

Fig. 7 – EIS of the passive films on 316L stainless steel in H_2SO_4 solution with different pH values at 25 °C.

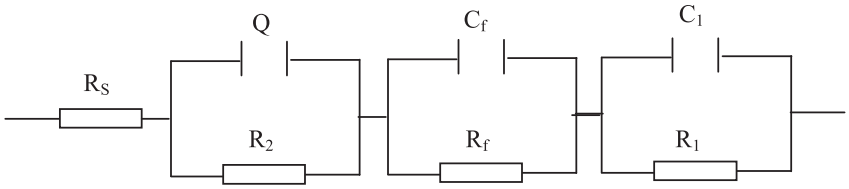

Fig. 8 – Equivalent circuit (R_s–(R_2//CPE)–(R_f//C_f)–(R_1//C_1)) used for fitting the EIS spectra.

representing the resistive contributions of the film/solution interface, it can be concluded that the increment of pH value can increase the resistance of the film/solution interface.

The capacitance of the film/solution interface, C, can be acquired by calculating the effective capacitance with a CPE [27]:

$$C = Q^{\frac{1}{\alpha}}\left(\frac{1}{R_s}+\frac{1}{R_2}\right)^{\frac{\alpha-1}{\alpha}} \quad (2)$$

For passive alloys in relative concentrated solutions, $R_2 >> R_s$ and Eq. (2) can be simplified to Eq. (3).

$$C = Q^{\frac{1}{\alpha}}R_s^{\frac{1-\alpha}{\alpha}} \quad (3)$$

Herewith, Fig. 9 shows the capacitances of the film/solution interface as the function of pH value in H_2SO_4 solution at 25 °C. It can be seen that $C_{f/s}$ sharply decreases with increasing pH value, it implies the enhanced difficulty of ions transfer from solution/film interface into the film, and hence to improve the film growth, it is consistent with the XPS.

Influence of pH value on Mott–Schottky plots of the passive film on 316L at 0.6 V for 24 h in H_2SO_4 solution

Before discussing the influences of pH value on the Mott–-Schottky plots of the passive films on 316L SS, it is necessary to clarify which frequency is selected to measure Mott–Schottky plot. The fitted EIS results shown in Table 3 propose the constant phase element (Q), which is an indication of the obvious dependence of the capacitance of the passive film on the measured frequency. In order to gain more information about the ionic properties of the passive film, Fig. 10 presents the typical $C \sim f$ plots for the steady-state films formed and measured at 0.6 V_{SCE} in the sulfuric acid solution. It is seen that the frequency-dependence behavior of the measured capacitance is different in two frequency regions. In the high frequency region (f > 100 Hz), the measured capacitance values are almost constant; whereas in the low frequency region (f < 100 Hz), all capacitances curves are shifted to higher values, which indicates that the capacitance dependence on the frequency in the low frequency region. Therefore, the frequency of 1 KHz is used as the applied frequency to eliminate the capacitance dependence on the frequency in this paper.

The semi-conductive property of the passive film on metal is often studied using the Mott–Schottky analysis based on the measurement of the electrode capacitance as a function of the applied potential. The reciprocal of the square of the capacitance (C) and the applied potential (E) exhibits a linear relationship under the depletion conditions.

For an n-type semiconductor [14,28–31]:

$$C^{-2} = \frac{2}{\varepsilon\varepsilon_0 e N_D}\left(E - E_{FB} - \frac{KT}{e}\right) \quad (4)$$

For a p-type semiconductor:

$$C^{-2} = -\frac{2}{\varepsilon\varepsilon_0 e N_A}\left(E - E_{FB} + \frac{KT}{e}\right) \quad (5)$$

Where e is the electron charge (1.602×10^{-19} C), N_D is the donor density, N_A is the acceptor density, ε is the dielectric constant of the passive film, taken as 15.6 [32]. ε_0 is the vacuum permittivity (8.854×10^{-14} F/cm), K is the Boltzmann constant (1.38×10^{-23} J/k), T is the absolute temperature and E_{FB} is the flat band potential. The KT/e term can be neglected because it is only approximately 25 mV at room temperature. From Eqs. (5) and (6), N_D and N_A can be determined from the slope of the plot of the experimental C^{-2} as a function of E, and E_{FB} can be obtained from extrapolation of the linear portion to $C^{-2} = 0$.

Fig. 11 shows the Mott–Schottky plots for the passive films formed on 316L SS at 0.6 V_{SCE} for 24 h in pH1 H_2SO_4 solution, which is measured by sweeping in both positive and negative directions. It is seen that there are few differences between the two curves, the two MS plots almost overlap in the whole potential region Therefore, the MS plots measured in the positive direction are used to explain the semi-conductive properties of the passive films on 316L SS. Based on the

Table 3 – Fit parameters for equivalent circuits corresponding to EIS measurements of 316L SS in H_2SO_4 solution with different pH values at 25 °C.

Solutions	$R_s/\Omega\cdot cm^2$	$Q/\Omega^{-1}\cdot s^{\alpha}$	α	$R_2/\Omega\cdot cm^2$	$C_f/F\cdot cm^{-2}$	$R_f/\Omega\cdot cm^2$	$C_1/F\cdot cm^{-2}$	$R_1/\Omega\cdot cm^2$	$\Sigma R/\Omega\cdot cm^2$	$\Sigma\chi^2$
pH = 1	12.64	4.475e-5	0.9126	1.157e6	2.627e-5	11.53	1.204e-5	6.701	1.157e6	7.361e-5
pH = 2	80.7	5.205e-5	0.7936	1.595e6	4.516e-5	1476	2.627e-5	1.129e5	1.708e6	7.508e-4
pH = 3	609.5	2.435e-5	0.8856	2.715e6	1.311e-5	3415	2.733e-5	595.9	2.715e6	9.886e-3
pH = 4	1480	3.716e-5	0.8995	3.451e6	4.143e-5	79.97	2.096e-5	5.357	3.451e6	1.91e-3
pH = 5	2440	2.863e-5	0.8491	2.145e6	7.14e-5	42.13	1.708e-6	1.374e6	3.519e6	1.634e-4
pH = 6	3810	1.871e-5	0.8927	4.166e6	2.421e-5	158.7	2.316e-6	2413	4.166e6	2.634e-4

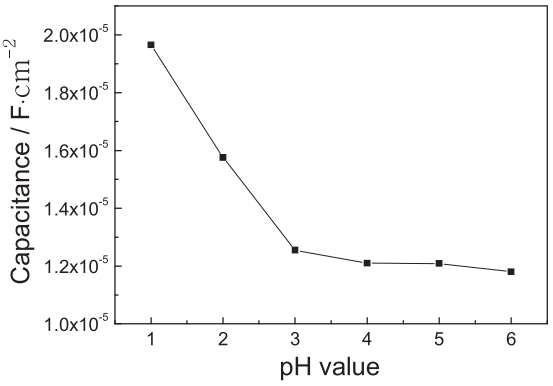

Fig. 9 – Capacitance of the film and solution interface verse pH value plot for 316L SS in H_2SO_4 solution.

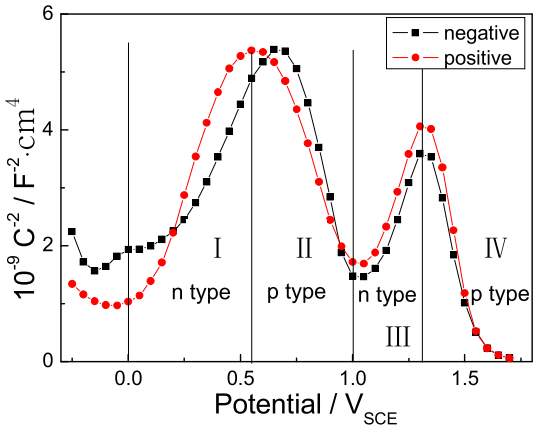

Fig. 11 – Mott–Schottky plots of the passive films on 316L SS at 0.6 V for 12 h in pH1 H_2SO_4 solution at 25 °C, the Mott–Schottky plots were measured by in the positive and negative directions.

slopes of the MS plots shown in Fig. 11, the MS plots can be divided into four regions, i.e., regions I(0 V_{SCE} ~ 0.55 V_{SCE}), II(0.55 V_{SCE} ~ 1.0 V_{SCE}), III(1.0 V_{SCE} ~ 1.3 V_{SCE}) and IV(1.3 V_{SCE} ~ 1.5 V_{SCE}). From 0 V_{SCE} to 0.55 V_{SCE}, the passive film on the specimen performs n-type semi-conductive property. When the potential range between 0.55 V_{SCE} and 1.0 V_{SCE}, the plots also show a linear tendency with a negative slope, indicating the p-type semi-conductive character. When the potential existing between 1.0 V_{SCE} and 1.3 V_{SCE}, a linear MS plot with the positive slope appears, suggesting the n-type semi-conductive character. When the applied potential falls into the range of 1.3 V_{SCE} and 1.5 V_{SCE}, the plots show a linear tendency with a negative slope, implying the p-type semi-conductive character. Fig. 12 depicts the Mott–Schottky plots of the passive films on 316L SS at 0.6 V for 24 h in the sulfuric acid solution with different pH values, it is obviously seen that the passive films in the cases of pH1, 2 and 3 perform good Schottky response, the Schottky response becomes weak as the pH value increasing to 4 and 5, it can be related to the changing of the film composition with pH value. The slopes of MS plots in the above four potential regions obviously increase with increasing pH value, implying the decrease in doping density of the passive film with pH value, the decrement of doping density is beneficial for the enhancement of anti-corrosion performance of passive film. With the applied potential moving from negative to positive direction (0 V_{SCE}~1.5 V_{SCE}), the slope of the Mott–Schittky plot varies with the positive-negative-positive values, which implies the passive film has the p-n heterojunction, similar results are obtained in other papers [33–36]. The dependence of Mott–-Schottky plot on the pH value can be attributed to the different chemical composition of the passive film formed on different potential range, the n-type oxide films Fe_2O_3 and $Fe(OH)_3$ [37] are probably formed in potential region I. With the increment of potential into region II, p-type Cr_2O_3 can be deposited on the sample surface. When the potential falls into the potential region III, some deep doping levels appearing n-type property may be produced. As the potential continues to increase, the dissolution of passive films occurs, Fe-oxides and Ni-oxides disappear in the passive film, simultaneously, the Cr_2O_3 content in the passive film sharply decreases, and a weak Schottky response is observed in this potential region. The above XPS results show that the Cr_2O_3 content in the

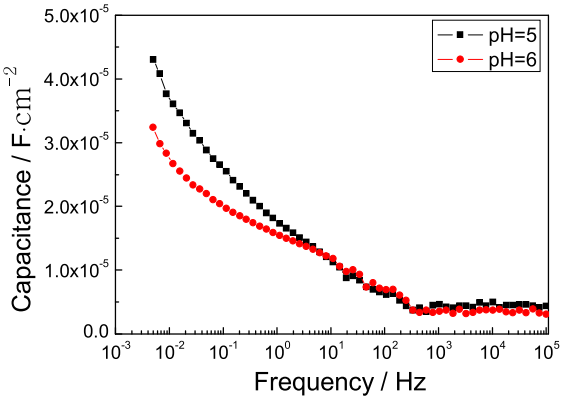

Fig. 10 – Capacitance vs. frequency curves for the steady-state passive film on 316L SS in H_2SO_4 solution at 0.6 V_{SCE} for 24 h.

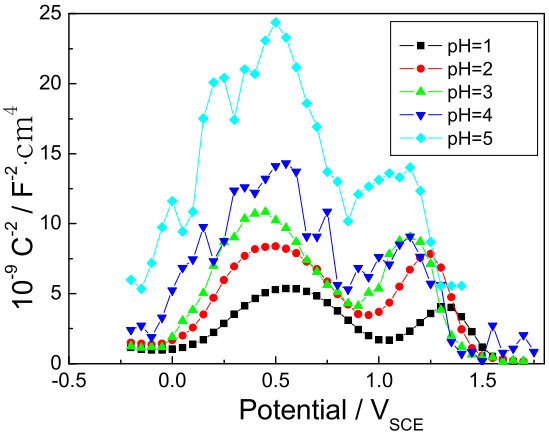

Fig. 12 – Mott–Schottky plots of the passive films on 316L SS at 0.6 V for 24 h in H_2SO_4 solution with different pH values at 25 °C.

Table 4 – The calculated parameters of the measured Mott–Schottky plots of the passive films formed on 316L SS at 0.6 V_{SCE} for 24h in H_2SO_4 solution. $N_{D,I}$, the donor density of the passive film in potential region I; $N_{A,II}$, the acceptor density of the passive film in potential region II; $N_{D,III}$, the donor density of the passive film in potential region III; $N_{A,IV}$, the acceptor density of the passive film in potential region IV; E_{FB}, the flat band potential.

Specimens	$N_{D,I}/cm^{-3}$	$N_{A,II}/cm^{-3}$	$N_{D,III}/cm^{-3}$	$N_{A,IV}/cm^{-3}$	E_{FB}/V_{SCE}
pH = 1	6.775×10^{20}	6.779×10^{20}	7.232×10^{20}	4.176×10^{20}	−0.113
pH = 2	3.552×10^{20}	5.307×10^{20}	3.837×10^{20}	2.045×10^{20}	−0.083
pH = 3	3.218×10^{20}	4.406×10^{20}	3.518×10^{20}	1.937×10^{20}	−0.098
pH = 4	1.225×10^{20}	4.127×10^{20}	2.803×10^{20}	2.009×10^{20}	−0.075
pH = 5	2.47×10^{20}	2.523×10^{20}	2.785×10^{20}	1.921×10^{20}	−0.067

passive film decreases and Fe-oxides content increases with the increment of pH value, therefore, the Schottky response becomes weak in the total potential region when the pH valve is over 3.

The donor density for n-type semi-conductive passive film, N_D; the acceptor density for p-type semi-conductive passive film, N_A; and the flat band potential, E_{FB}, can be calculated by the connection of Fig. 12, formulas (4) and (5). The calculated results are showed in Table 4, it can be observed that the order of the magnitude of the donor and acceptor densities reaches to 10^{20} ~ 10^{21} cm^{-3}, and the doping densities significantly decrease with the increment of pH value. A higher concentration of donor or acceptor density in the passive film should improve the pitting tendency of the substrate [38], hence, it can be concluded that the increase in pH value can decrease the pitting susceptibility of 316L SS via decreasing the donor and acceptor densities of the passive films.

The flat band potential (E_{FB}) is a critical parameter used to determine the positions of the semiconductor energy bands with respect to the redox potentials of electro active ions in the solution, and it provides useful information to understanding the localized corrosion resistance although the flat band potential is complicated by the presence of surface states and defects unavoidably connected with the nanometer size of the passive film [39–41]. Table 4 shows that the flat band potential moves to positive direction with increasing pH value, suggesting the increment of the passive film stability [40].

Conclusions

The influence of pH value on the structure and the electronic property of the passive film on 316L SS in the simulated cathodic environment of the proton exchange membrane fuel cell, were explored using potentiodynamic polarization curve, electrochemical impedance spectra (EIS), Mott–Schottky plot and X-ray photoelectron spectroscopy (XPS). The following conclusions can be drawn as following:

1) The increment of pH value can appreciably lower the passive current density and enhance the polarization resistance of 316L SS in the simulated cathodic environment of PEMFC, and hence to improve its anti-corrosion behavior;
2) pH value had a markedly influence on the composition and structure of the passive films formed on 316L SS, the passive film was mainly composed of the inner Fe-rich oxide and the outer Cr-oxide when the pH value was below 3. Fe-oxide became the major component and Cr-oxide content became weak with increasing pH value when the pH value was over 3;
3) The increment of pH value can enhance the protectiveness of the passive films on 316L SS by increasing transfer resistance of charge between the film/solution interface by means of improving the compactness of the passive film and increasing film thickness;
4) The passive film on 316L SS appeared the p-n heterojunction structure, the donor and acceptor densities was in the order of the magnitude of 10^{20} cm^{-3}, and they significantly decreased with the increment of pH value, simultaneously, the flat band potential moved to positive direction with pH value.

Acknowledgment

This work is financially supported by the National Nature Science Foundation of China (No. 51305228).

REFERENCES

[1] Bar IO, Kirchaina R, Roth R. J Power Sources 2002;109:71–5.
[2] Tsuchiya H, Kobayashi O. Int J Hydrogen Energy 2004;29:985–90.
[3] Antunes RA, Oliveira MCL, Ett G, Ett V. Int J Hydrogen Energy 2010;35:3632–47.
[4] Wang H, Sweikart MA, Turner JA. J Power Sources 2003;115:243–51.
[5] Makkus RC, Janssen AHH, De Bruijn FA, Mallant RKAM. J Power Sources 2000;86:274–82.
[6] Davies DP, Adcock PL, Turpin M, Rowen SJ. J Power Sources 2000;86:237–42.
[7] Wang Y, Northwood DO. Electrochim Acta 2007;52:6793–8.
[8] Lafront AM, Ghali E, Morales AT. Electrochim Acta 2007;52:5076–85.
[9] Boissy C, Dumont CA, Normand B. Electrochem Commun 2013;26:10–2.
[10] Feng K, Wu GS, Li ZG, Cai X, Chu PK. Int J Hydrogen Energy 2011;36:13032–42.
[11] Shintani D, Ishida T, Lzumi H. Corros Sci 2008;50:2840–5.
[12] Montemor MF, Ferreira MGS. Corros Sci 2000;42:1635–50.
[13] Ferreira MGS, Dawson JL. J Electrochem Soc 1985;132:760.
[14] Hakiki NE, Da Cunha Belo M, Smiões AMP, Ferreira MGS. J Electrochem Soc 1998;145:3821.

[15] Taveira LV, Montemor MF, Da Cunha Belo M, Ferreira MG, Dick LFP. Corros Sci 2010;52:2813–8.
[16] Jüttner K. Electrochim Acta 1990;35:1501.
[17] Ameer MA, Fekry AM, Taib Heakal FEI. Electrochim Acta 2004;50:43.
[18] Priyantha N, Jayaweera P, Macdonald DD, Sun A. J Electroanal Chem 2004;572:409.
[19] Lukacs Z. J Electroanal Chem 1997;432:79.
[20] Lukacs Z. J Electroanal Chem 1999;464:68.
[21] Young L. Anodic oxide films. New York: Academic Press; 1961.
[22] Schiller CA, Strunz W. Electrochim Acta 2001;46:3619.
[23] Jurczakowski R, Hitz C, Lasia A. J Electroanal Chem 2004;572:355.
[24] Pajkossy T. Solid State Ionics 2005;176:1997.
[25] Brug GJ, van den Eeden ALG, Sluyters-Rehbach M, Sluyters JH. J Electroanal Chem 1984;176:275.
[26] Lasia A. In: Modern aspects of electrochemistry. New York: Plenum Press; 1999.
[27] Clayton CR, Lu JC. Corros Sci 1989;27:881.
[28] De Gryse R, Gomes WP, Cardon F, Vennik J. J Electrochem Soc 1975;122:711.
[29] Finklea HO. J Electrochem Soc 1982;129:2003.
[30] Hakiki NE, Da Cunha Belo M. J Electrochem Soc 1996;143:3088.
[31] Nogami G. J Electrochem Soc 1982;129:2219.
[32] Di Paola A. Electrochim Acta 1989;34:203.
[33] Hakiki NE, Boudin S, Rondot B, Da Cunha Belo M. Corros Sci 1995;37:1809.
[34] Di Paola A, Shukla D, Stimming U. Electrochim Acta 1991;36:345.
[35] Ries LAS, Da Cunha Belo M, Ferreira MGS, Muller IL. Corros Sci 2008;50:968.
[36] Da Cunha Belo M, Hakiki NE, Ferreira MGS. Electrochim Acta 1999;44:2473.
[37] Azumi K, Ohtsuka T, Sato N. J Electrochem Soc 1987;134:1352.
[38] Zeng YM, Luo JL. Electrochim Acta 2003;48:3551.
[39] Harrington SP, Devine TM. J Electrochem Soc 2009;156:C154.
[40] Schmidt AM, Azambuja DS, Martini EMA. Corros Sci 2006;48:2901.
[41] Sikora E, Sikora J, Macdonald DD. Electrochim Acta 1996;41:783.